Journal of Biomechanics 43 (2010) 210–220

Contents lists available at ScienceDirect

Journal of Biomechanics

journal homepage: www.elsevier.com/locate/jbiomech
www.JBiomech.com

A numerical model of cellular blebbing: A volume-conserving, fluid–structure interaction model of the entire cell

Jennifer Young *, Sorin Mitran

University of North Carolina at Chapel Hill, Department of Mathematics, CB #3250, Phillips Hall, Chapel Hill, NC 27599, USA

ARTICLE INFO

Article history:
Accepted 2 September 2009

Keywords:
Bleb
Fluid–structure interaction
Volume constraint
Actin
Cytoskeleton

ABSTRACT

In animal cells, blebs are smooth, quasi-hemispherical protrusions of the plasma membrane that form when a section of the membrane detaches from the underlying actin cytoskeleton and is inflated by flowing cytosol. The mechanics behind this common cellular activity are not yet clear. As a first step in the development of a full computational framework, we present a numerical model of overall cell behavior based upon the interaction between a background Newtonian-fluid cytosol and elastic structures modeling the membrane and filaments. The detailed micromechanics of the cytoskeletal network are the subject of future work. Here, the myosin-driven contraction of the actin network is modeled through stressed elastic filaments. Quantitative models of cytoskeletal micromechanics and biochemistry require accurate estimates of local stress and flow conditions. The main contribution of this paper is the development of a computationally efficient fluid–structure interaction model based on operator splitting, to furnish this data. Cytosol volume conservation (as supported by experimental evidence) is enforced through an intermediate energy minimization step. Realistic bleb formation and retraction is observed from this model, offering an alternative formulation to positing complex continuum behavior of the cytoplasm (e.g. poroelastic model of Charras et al., 2008).

1. Introduction

In animal cells, a bleb is a fluid-filled protrusion that forms when the plasma membrane separates from the underlying actin cytoskeleton (Charras et al., 2005; Dai and Sheetz, 1999; Sheetz et al., 2006), and is pushed outward by pressure-driven cytosol (Albrecht-Buehler, 1982; Charras et al., 2005; Cunningham, 1995; Erickson and Trinkaus, 1976). Blebbing occurs during apoptosis (Charras et al., 2005; Mills et al., 1998; Sheetz et al., 2006), mitosis (Albrecht-Buehler, 1982; Dai and Sheetz, 1999; Erickson and Trinkaus, 1976), and cell spreading and motility (Charras et al., 2005; Cunningham, 1995; Dai and Sheetz, 1999). During bleb formation and retraction, the overall cellular volume remains constant (Albrecht-Buehler, 1982; Charras et al., 2005; Cunningham, 1995). The biomechanical process behind the phenomenon is not yet completely understood. There are several topics under discussion in the literature (Charras, 2008), including how to characterize the cell's cytoskeleton. One viewpoint posits the actin cortex to be a continuous medium, either as a poroelastic material (Charras et al., 2008) or as a highly viscous fluid (Alt and Dembo, 1999). The continuum hypothesis excludes consideration of anisotropic microdynamics taking place within the cytoskeleton (Yoon et al., 2008). We present here an alternative modeling approach that couples the motion of a Newtonian fluid (the cytosol) with the deformation of elastic structures (the membrane and filaments). This volume conserving, fluid–structure interaction model lays the groundwork for a full, micromechanical computation of cytoskeletal dynamics to be presented in future work.

A number of computational models have been made to simulate protrusive activities in cells. Bottino and Fauci (1998) used an immersed boundary method to model directed motion in crawling cells. Alt and Dembo (1999) took a two-phase fluid approach to cell locomotion, treating both the actin filament cortex and the cytosol as viscous fluids. A system of generalized Stokes equations with Darcy's law was used to model the fluid flow, including the transition between the two fluid phases. With respect to previous work, our model includes additional features such as a volume constraint to ensure accurate computation of fluid variables, the dynamic elastic stresses of the membrane, and a framework conducive to a forthcoming micromechanics description of the cytoskeleton.

1.1. Biological background

1.1.1. Cellular structures

The cellular structures thought to be involved in bleb formation are the actin cytoskeleton, the cytosol, and the plasma

* Corresponding author. Tel.: +1 302 593 6286; fax: +1 919 962 2568.
E-mail address: jendjoy@email.unc.edu (J. Young).

0021-9290/$ - see front matter © 2009 Elsevier Ltd. All rights reserved.
doi:10.1016/j.jbiomech.2009.09.025

membrane. The actin cytoskeleton is the peripheral, mesh-like structure composed primarily of cross-linked actin filaments which gives the cell its mechanical strength and shape (Alberts et al., 2002; Boal, 2002). Motor protein polymers, myosin II, can be found interlaced among the actin filaments and are capable of producing contractile forces within the cytoskeleton (Alt and Dembo, 1999). A typical cytoskeleton contains 100,000–400,000 actin filaments (Boal, 2002; Cano et al., 1991), with each 8 nm thick fiber ranging in length from 0.2 to 20 μm (Boal, 2002; Cano et al., 1991; Janmey et al.,).

The cytosol is the fluid within the cell (Boal, 2002; Bray, 2000). It comprises water and dissolved proteins (Bray, 2000) with a viscosity of 1.1–3.0 cP (Bicknese et al., 1993; Mastro et al., 1984). The fluid pressure inside the cell is normally 20–300 Pa higher with respect to that of the external ambient fluid (Charras et al., 2008; Rand and Burton, 1964).

The plasma membrane is a 4–5 nm thick, semi-permeable lipid bilayer that encases the actin cortex and cytoplasm (Alberts et al., 2002; Boal, 2002). The plasma membrane can only stretch 2–5% of its area before rupturing (Evans and Skalak, 1980; Morris and Homann, 2001; Sheetz et al., 2006). However, a cell houses extra membrane surface area in folds, ruffles, microvilli and internal vacuole-like dilations to accommodate possible shape changes (Dai and Sheetz, 1999; Erickson and Trinkaus, 1976; Evans and Yeung, 1989; Herring et al., 1999; Schmid-Schönbein et al., 1980; Sheetz et al., 2006). The plasma membrane and cytoskeletal filaments are attached together via interactions with transmembrane proteins often mediated by adaptor proteins, as well as via interactions with lipids (Alberts et al., 2002).

1.1.2. Blebs

Once a segment of membrane and cytoskeleton have separated, blebs take 3–10 s to fully expand (Albrecht-Buehler, 1982; Charras et al., 2005; Cunningham, 1995). Their sizes range from 5 to 125 μm^3 (about 0.003–15% of the overall cell volume) (Albrecht-Buehler, 1982; Cunningham, 1995) but they can be larger for cells undergoing apoptosis (Sheetz et al., 2006). A bleb usually remains expanded for 10–20 s and then slowly retracts for 30–60 s (Cunningham, 1995; Dai and Sheetz, 1999). Retraction occurs due to the formation and subsequent myosin-driven contraction of a new actin mesh on the inside rim of the bleb (Charras et al., 2006; Keller and Eggli, 1998). This new cortex is built from protein monomers recruited from the fluid within the bleb (Charras et al., 2006).

The initial membrane–cytoskeleton detachment is hypothesized to be due to a myosin II-driven contraction within the actin mesh (Charras et al., 2006; Pullarkat, 2006), creating a force that breaks the adhesive bonds. At the site of bleb formation the plasma membrane morphs smoothly (Cunningham, 1995; Dai and Sheetz, 1999), unfurling local folds and invaginations to provide for this shape change (Dai et al., 1998; Erickson and Trinkaus, 1976; Schmid-Schönbein et al., 1980; Sheetz et al., 2006).

The overall cellular volume remains constant during bleb formation and retraction (Albrecht-Buehler, 1982; Charras et al., 2005; Cunningham, 1995). This supports the hypothesis that it is an internal fluid–membrane interaction driving bleb expansion (Albrecht-Buehler, 1982; Charras et al., 2005; Cunningham, 1995), and excludes the possibility of external fluid flow moving across the membrane into the bleb (Cunningham, 1995). Actin polymerization does not play a role in bleb formation (Cunningham, 1995). There is visual evidence of the lack of actin in growing blebs (Albrecht-Buehler, 1982; Charras et al., 2006). Fig. 1 lists the sequence of assumptions utilized in this model.

2. Model development

2.1. Mathematical equations

We present here the equations for a two-dimensional model of bleb formation and retraction. A two-dimensional model was chosen due to the protrusion's approximate radial symmetry.

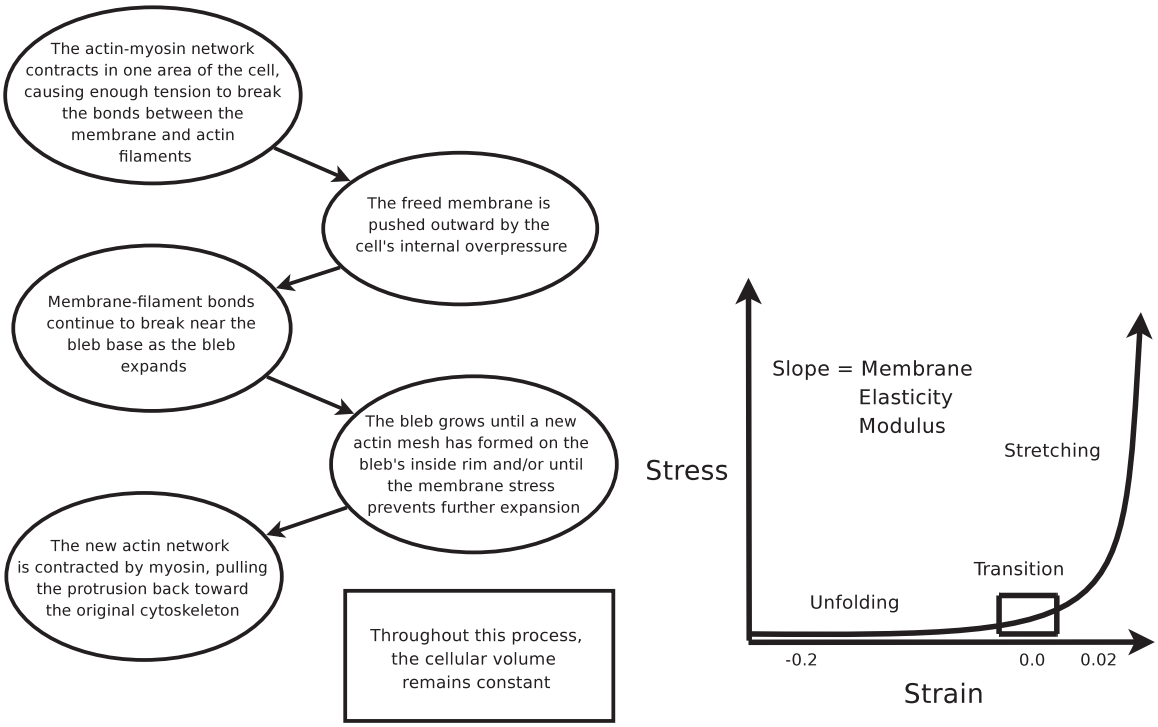

Fig. 1. Sequence of model assumptions for a blebbing scenario (left) and a schematic graph of the stress–strain relationship of the plasma membrane (right).

2.1.1. Actin filaments

The cytoskeleton is a complex structure composed of approximately 10^5 cross-linked filaments (Boal, 2002). We are currently constructing a detailed micromechanical network description of the cytoskeleton to be presented in future work. Here, we consider the average effect of the cytoskeleton upon the blebbing phenomenon, which appears in the form of filament forces imposed on the membrane.

Due to their length scale and mechanical properties (Janmey et al.,), actin filaments are modeled as one-dimensional, elastic strings. Their forces are computed via Hooke's Law and added as external forces to the membrane equation. Two types of filament forces are present in this model: (1) regular filament forces at the cell's periphery that model the membrane–cytoskeleton attachments and (2) retraction filament forces that occur inside the bleb as a myosin-driven contractile force on the protruded membrane.

2.1.2. Monomer concentrations

In accordance with experimental evidence, retraction occurs when protein monomers present in the cytosol are polymerized into filamentous actin and myosin polymers to form a new cortex (Charras et al., 2006). These protein subunits diffuse (Kolega and Taylor, 1993; Zicha et al., 2003) and are advected (Zicha et al., 2003) into the bleb by the locally surrounding fluid. We include the motion of these protein molecules via advection–diffusion equations:

$$q_t + uq_x + vq_y = \alpha(q_{xx} + q_{yy}) + \phi(q)$$

where q is the free monomer concentration, u and v are the local fluid velocities and α is the diffusion coefficient (see Fig. 3 for coefficient values). The term $\phi(q)$ represents the transition of monomers to the polymer state or vice versa, depending on polymerization and depolymerization rates. In blebbing, $\phi(q)$ is mainly a sink term representing the net loss of monomers that get transformed into filament form within the protrusion.

2.1.3. Plasma membrane

Though the plasma membrane can be described by a fluid model (Alberts et al., 2002), micromechanical measurements by scanning force microscopy suggest that an elastic model with varying elasticity modulus is also valid (Künneke et al., 2004). Similar to the filament case (Boal, 2002; Dai and Sheetz, 1999; Nichol and Hutter, 1996; Rawicz et al., 2000), the lipid bilayer is represented as a one-dimensional elastic string. The membrane typically contains ruffles and invaginations which are unfurled to allow for cellular protrusions (Dai et al., 1998; Erickson and Trinkaus, 1976; Schmid-Schönbein et al., 1980; Sheetz et al., 2006). The presence of folds is modeled by a strain-dependent elasticity modulus. A wrinkled membrane segment is modeled by a compressed spring with a low, positive elasticity modulus representing the energy required to overcome small membrane bending moments ($\approx 10^{-19}$ J, Boal, 2002). This allows for large membrane displacements that create small material stress. Once the strain reaches zero this equates to the biological membrane being completely unfolded. As strain increases, the elasticity modulus increases by several orders of magnitude (Künneke et al., 2004) to represent the membrane's resistance to stretching. Fig. 1 shows a schematic of the membrane's stress–strain curve.

The motion of the membrane is modeled with a damped wave equation with forces from fluid pressure, viscosity, and the filaments added as source terms. Pressure pushes outward on the membrane, so this force is written as $\Delta p \cdot \mathbf{n}$ where p is pressure and $\mathbf{n}$ is the normal vector. The filament forces are computed from Hooke's law. The viscous forces are computed from the viscous stress tensor T that arises in the fluid equation. The membrane equation is

$$\lambda \boldsymbol{\delta}_{tt} = E\boldsymbol{\delta}_{SS} + \Delta p \cdot \mathbf{n} - \sum k(\Delta S \cdot \mathbf{n} + \Delta S \cdot \mathbf{t}) + \eta(T \cdot \mathbf{n} + T \cdot \mathbf{t})$$

where $\boldsymbol{\delta}$ is the two-dimensional displacement vector, S is arc length, t is time, λ is a linear mass density, E is the varying elasticity modulus, η is the fluid viscosity, k is the filament spring constant, ΔS is the filament length displacement from equilibrium and $\mathbf{t}$ is the membrane tangent vector. This is the equation of motion for the membrane when it is attached to the cytoskeleton. For a detached segment of membrane the filament force term is zero.

2.1.4. Cytosol

Blebs form due to the flow of pressurized cytosol (Albrecht-Buehler, 1982; Charras et al., 2005; Cunningham, 1995; Erickson and Trinkaus, 1976). The fluid found in expanding blebs is devoid of filament fragments (Charras et al., 2005), thus the cytosol is modeled as an incompressible Newtonian fluid. During blebbing the cytosol undergoes low Reynolds flow ($Re \approx 10^{-6}$) due to the cell's small length scale. The Stokes equations is utilized to solve for the fluid motion:

$$-\nabla p + \eta \Delta \mathbf{u} = 0$$

$$\nabla \cdot \mathbf{u} = 0$$

where $\mathbf{u}$ is the velocity vector.

2.2. Numerical methods

The numerical fluid–structure interaction problem is solved through the operator splitting approach outlined in Fig. 2. We have developed a publicly available software implementation based upon the Bearclaw framework for solving time dependent partial differential equations (PDEs) (Mitran, 2001).

2.2.1. Solution methods for the individual equations

To solve the hyperbolic elasticity portion of the membrane equation and the advection part of the concentration equations, we employ a wave propagation algorithm (LeVeque, 1997). The diffusion component of the concentration equations is solved with a Crank–Nicolson scheme. Source terms are incorporated into the solution of each equation via a fractional step method. The Stokes equations are recast in a vorticity-stream function formulation (Fletcher, 1988), and solved using a multigrid iterative scheme.

2.2.2. Grid generation

The cell is discretized with a curvilinear grid that is mapped to a Cartesian grid upon which all numerical procedures are carried out. A conformal, orthogonal grid allows for straightforward implementation of the numerical methods. Such a grid can be generated given the current cell boundary by solving a set of PDEs derived from the Euler–Lagrange variational principle (Jose and Saletan, 1998; Ryskin and Leal, 1983; Zhang et al., 2006). To make the grid truly orthogonal requires that the boundary points be allowed to "slide" along the boundary curve to orient themselves in orthogonally favorable positions that satisfy the Riemann mapping theorem (Bak and Newman, 1997). This results in a non-linear problem. To avoid the complications of a non-linear solve, we enforce orthogonality in the domain's interior and use general curvilinear grid mapping procedures to compute boundary conditions for the fluid equations.

2.2.3. Volume constraint

Biological experiments show that the fluid volume remains constant during blebbing (Albrecht-Buehler, 1982; Charras et al.,

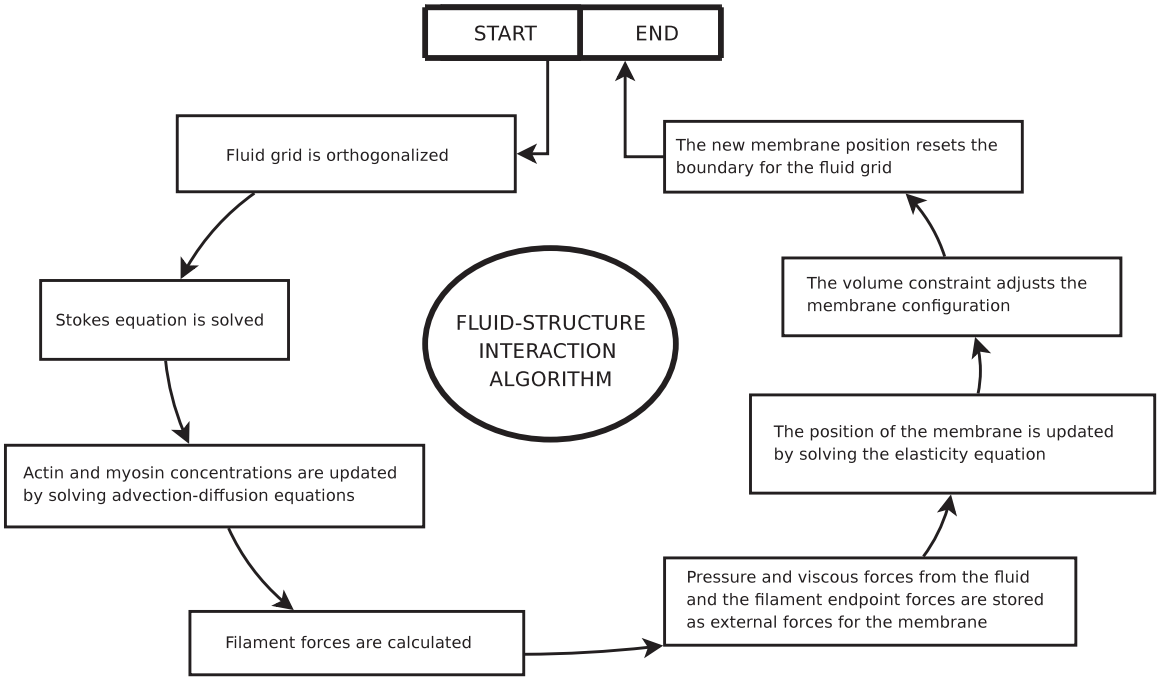

Fig. 2. The sequence of steps which occurs during one time step of the simulation.

2005; Cunningham, 1995). The operator splitting procedure employed in the simulation offers economy in computation but does not necessarily conserve volume. At a constant temperature, fluid stresses and volume are related, so any artificial changes in volume will cause an artificial change in fluid stress. To fix this issue, at an intermediate step in time advancement after the membrane has been moved to a new position, we apply Gauss' principle of least constraint to obtain a corrected membrane configuration (Papastavridis, 2002). Using the idea of Lagrange multipliers, we wish to minimize the following function:

$$L(x_i, y_i, \lambda) = E(x_i, y_i) + \lambda(V(x_i, y_i) - c)$$

where λ is the Lagrange multiplier, V is the current cell volume, c is the cell's initial volume that we wish to maintain, and x_i, y_i are the membrane coordinate points. The total energy E expended by the cell includes the elastic energy of the membrane and the work done by fluid pressure and filaments on the membrane. The solution to this minimization problem is found using a quasi-Newton method (Bertsekas, 1982).

Parameter	Value in SI units
Cell Diameter	10 μm
Regular Filament Equilibrium Length	3.4 μm
Regular Filament Strains	< 1%
Filament Spring Constant	20.5 pN/nm
Percentage of Excess Membrane	25%
Approximate Expansion Time	10 s
Approximate Stasis and Retraction Time	30 s
Total Number of Filaments in Model	1024
Filament/Membrane Detachment Rate	5 filaments/s
Bleb Diameter (fully expanded)	0.7 μm
Fluid Viscosity	1.3 cP
Pressure Difference across Membrane	103 Pa
Actin Diffusion Coeffcient	10^{-8}cm^2/s
Myosin Diffusion Coeffcient	10^{-9}cm^2/s

Fig. 3. List of parameter values used in the simulation.

3. Results

We present results for a model cell. Parameter values (see Fig. 3) were chosen to be close to those found in the literature but do not model a particular cell type or scenario. The model can handle arbitrary initial membrane conformations and filament distributions. We chose a circular membrane with filaments equally distributed across the cell as a test case.

3.1. Model of bleb formation and retraction

At the start of the simulation, filaments are in an extended state, the membrane is compressed (wrinkled), and the pressure inside the cell is positive. A small number of adjacent filaments are released from the membrane in one area of the cell. During subsequent time steps, filaments at the edges of the freed membrane are released at a constant velocity. This velocity represents the average speed of membrane–filament detachment based on comparing the membrane–cytoskeleton adhesion energy (Sheetz, 2001) and the energy in the membrane at the edge of the bleb. As the freed membrane expands driven by fluid pressure, it entrains fluid that transports actin and myosin monomers into the bleb. At each time step, a percentage of these actin monomers are removed from the fluid and added to newly forming retraction filaments. This percentage parameter is determined from the difference in polymerization and depolymerization rates for an actin filament under the given monomer concentration. A similar procedure is carried out for myosin. Once a base cortex has been established, the retraction filaments become active, contractile springs within the model. These filaments collectively produce an inward force on the membrane. Figs. 4–7 show series of simulation time steps, displaying different variables such as fluid velocity, pressure, free actin monomer concentration, and the presence of filament forces.

Fig. 8 displays a graph of the total contractile force generated within the bleb as a function of the bound myosin concentration.

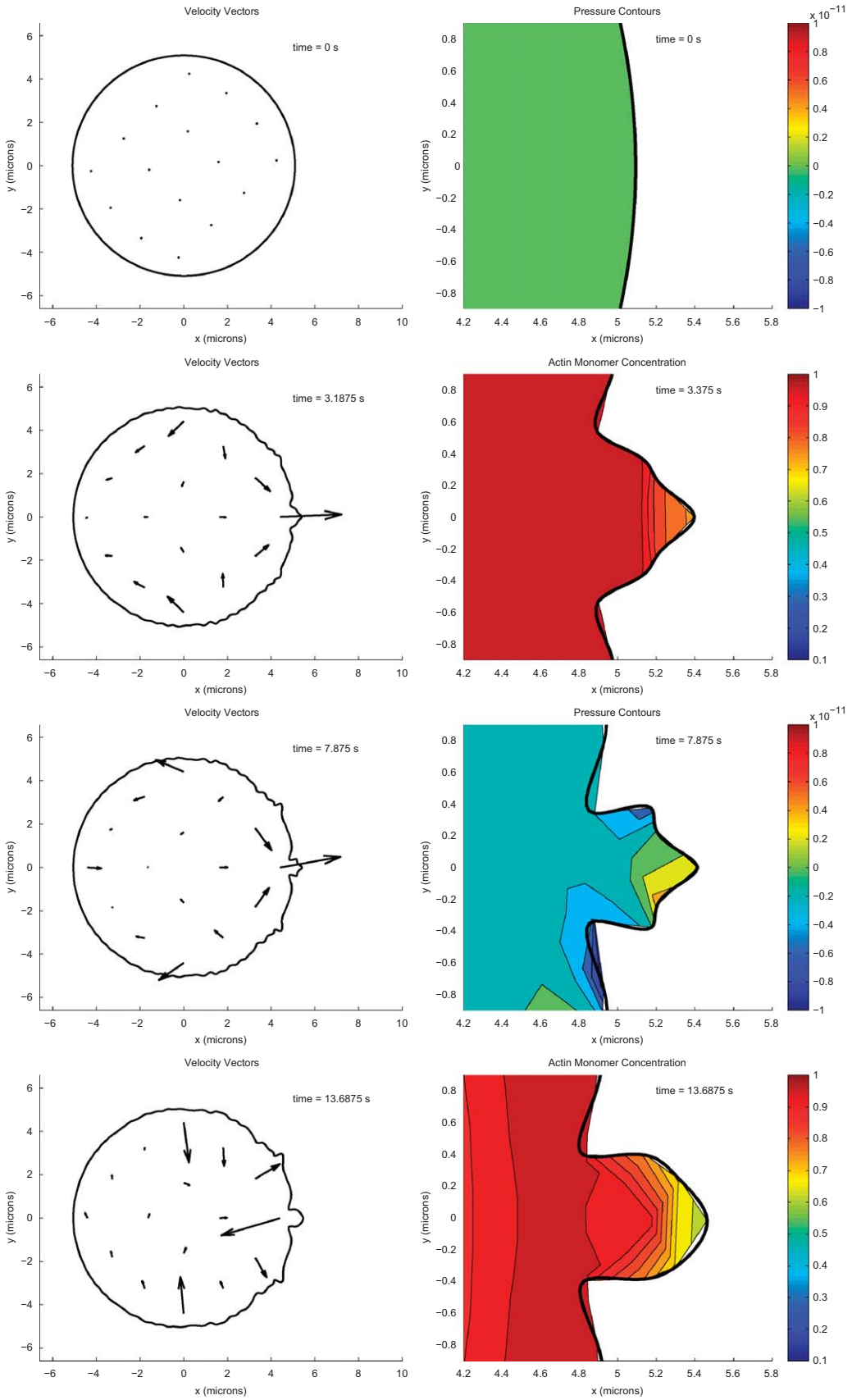

Fig. 4. A series of snapshots of the cell membrane as the bleb forms and retracts. The full cell figures (left) show fluid velocity vectors, while the zoom view figures (right) depict either the pressure contours or the free actin monomer concentration contours. Pressure values shown are the actual values minus the initial uniform pressure of 103 Pa. Note that the pressure is slightly higher inside the bleb during expansion, but drops to lower values during retraction. Also note that the free actin monomer concentration (in mg/ml) decreases in the bleb over time as the monomers are converted to filamentous actin.

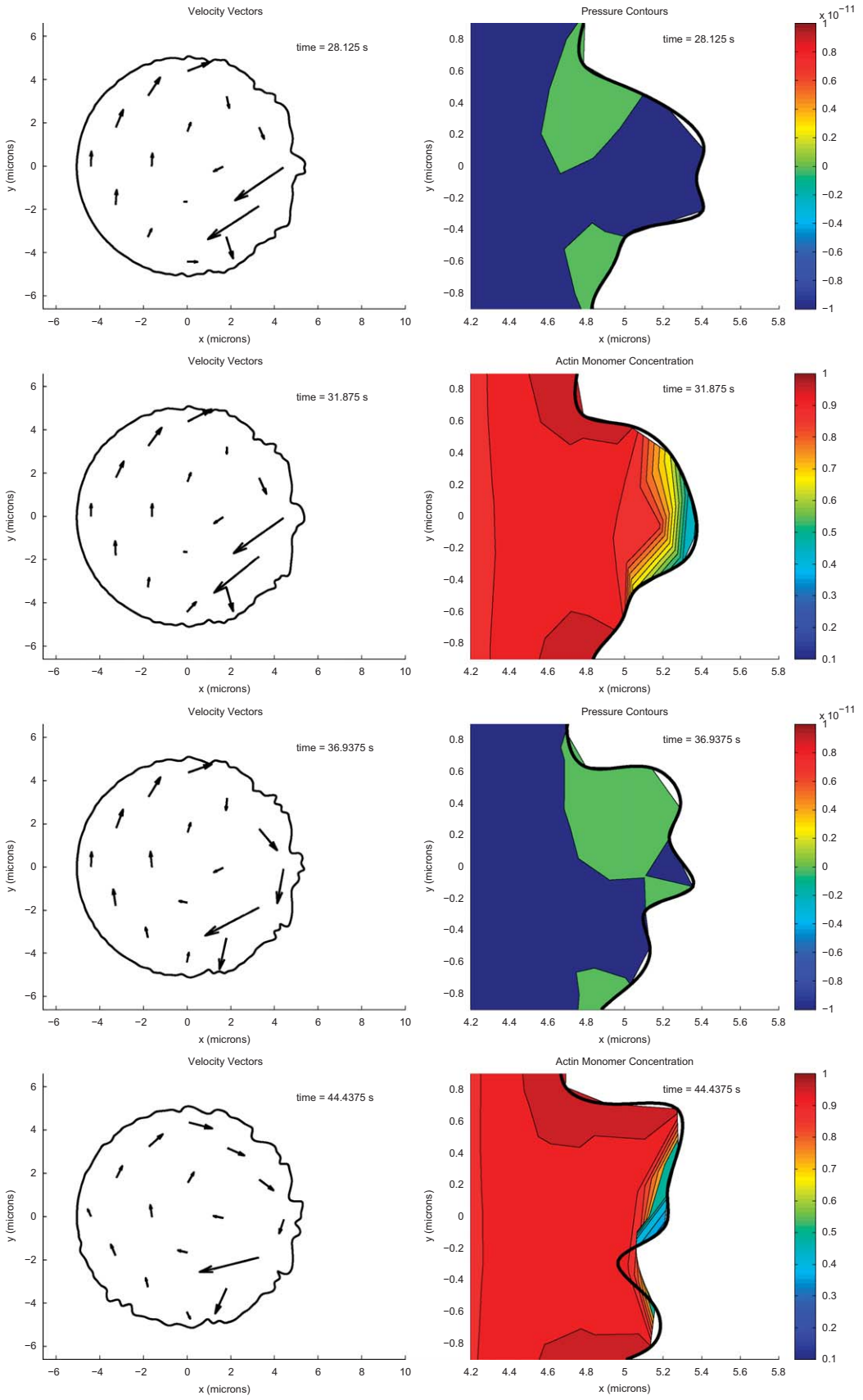

Fig. 5. A series of snapshots of the cell membrane as the bleb forms and retracts. The full cell figures (left) show fluid velocity vectors, while the zoom view figures (right) depict either the pressure contours or the free actin monomer concentration contours. Pressure values shown are the actual values minus the initial uniform pressure of 103 Pa. Note that the pressure is slightly higher inside the bleb during expansion, but drops to lower values during retraction. Also note that the free actin monomer concentration (in mg/ml) decreases in the bleb over time as the monomers are converted to filamentous actin.

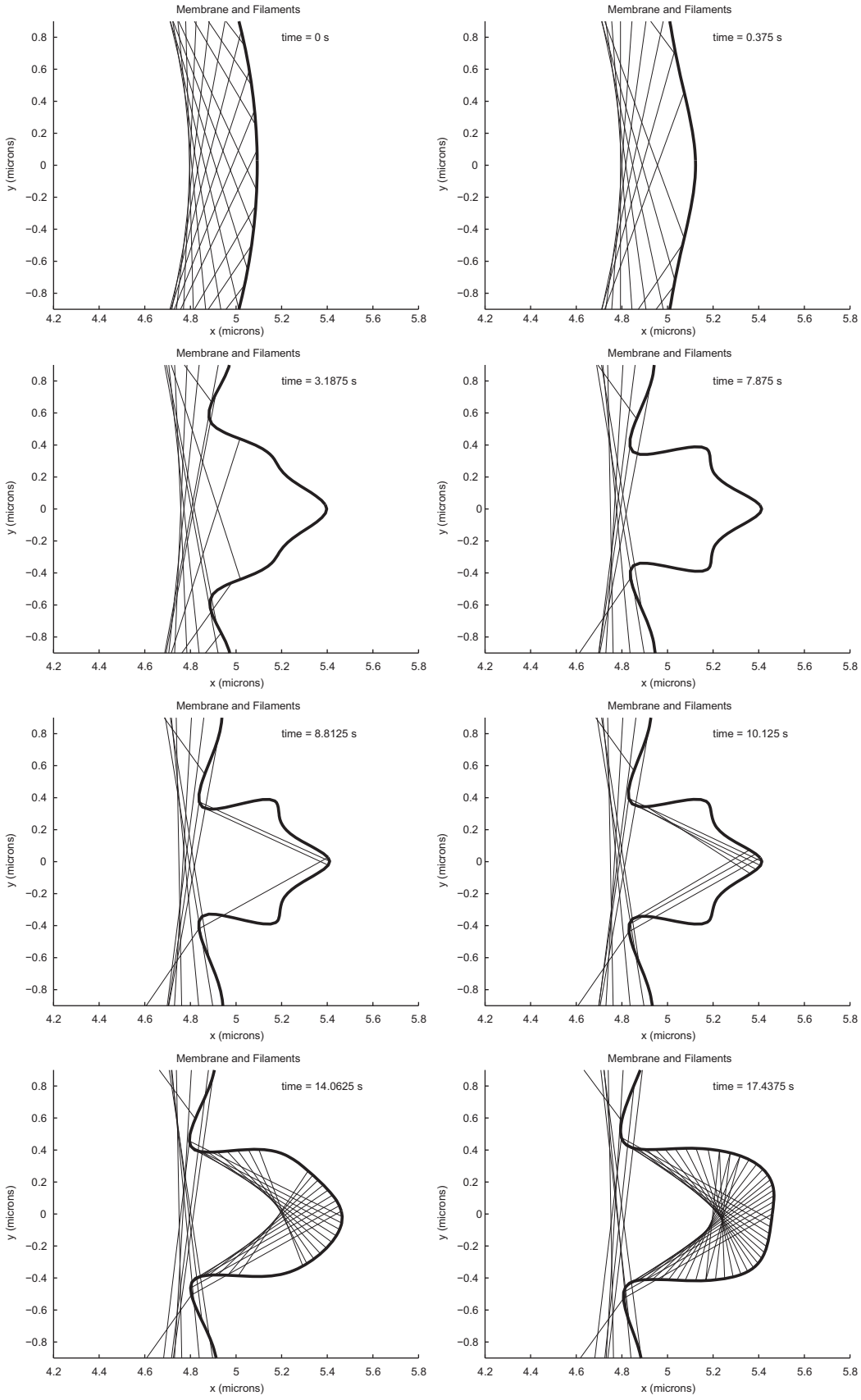

Fig. 6. A series of zoom view snapshots of the membrane and filament forces as the bleb forms and retracts. The filaments which appear in the later time steps within the bleb are there to represent the forces generated by the newly forming and contracting actin cortex.

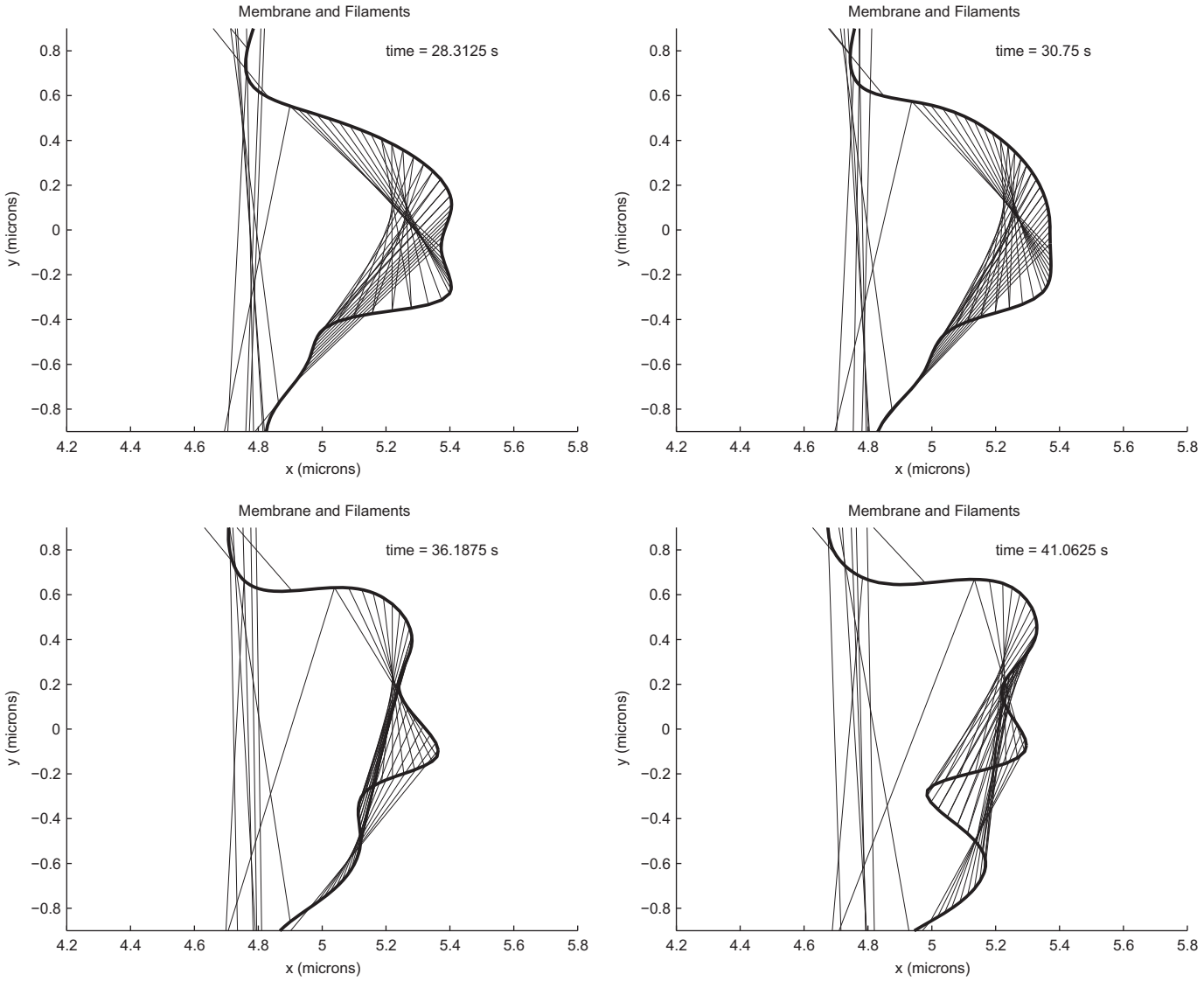

Fig. 7. A series of zoom view snapshots of the membrane and filament forces as the bleb forms and retracts. The filaments which appear in the later time steps within the bleb are there to represent the forces generated by the newly forming and contracting actin cortex.

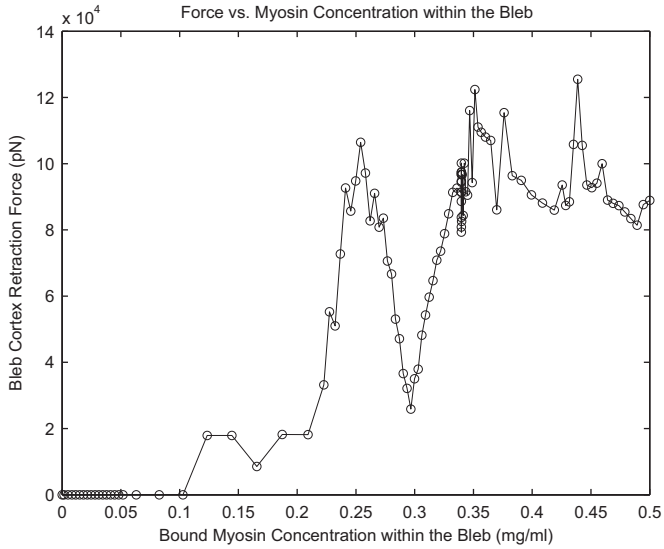

Fig. 8. The total force generated by the retracting bleb cortex versus the bound myosin concentration within the bleb.

Initially, there is no retraction force because the proteins have not yet built up enough within the bleb to form a basic cortex. Once thresholds have been reached, the new network begins to contract. As protein levels continue to increase, so does the total force. The variability in force seen later in the graph can be attributed to the fluctuating balance between the decreasing forces needed to pull the shrinking bleb inward versus the increasing amount of bound proteins.

3.2. Validation

The numerical implementation of the various equations of motion were individually validated by comparing the results against known analytical solutions for simpler problems. The curvilinear grid mapping was also tested to ensure that it produced reasonable grids for the fluid domain.

As a test of the volume constraint, conditions were created to induce bleb formation, and the program was run with and without the volume conservation procedure. In both cases, the volume of the initial membrane configuration was compared to the volume of the blebbed membrane. The results are displayed in Fig. 9. With

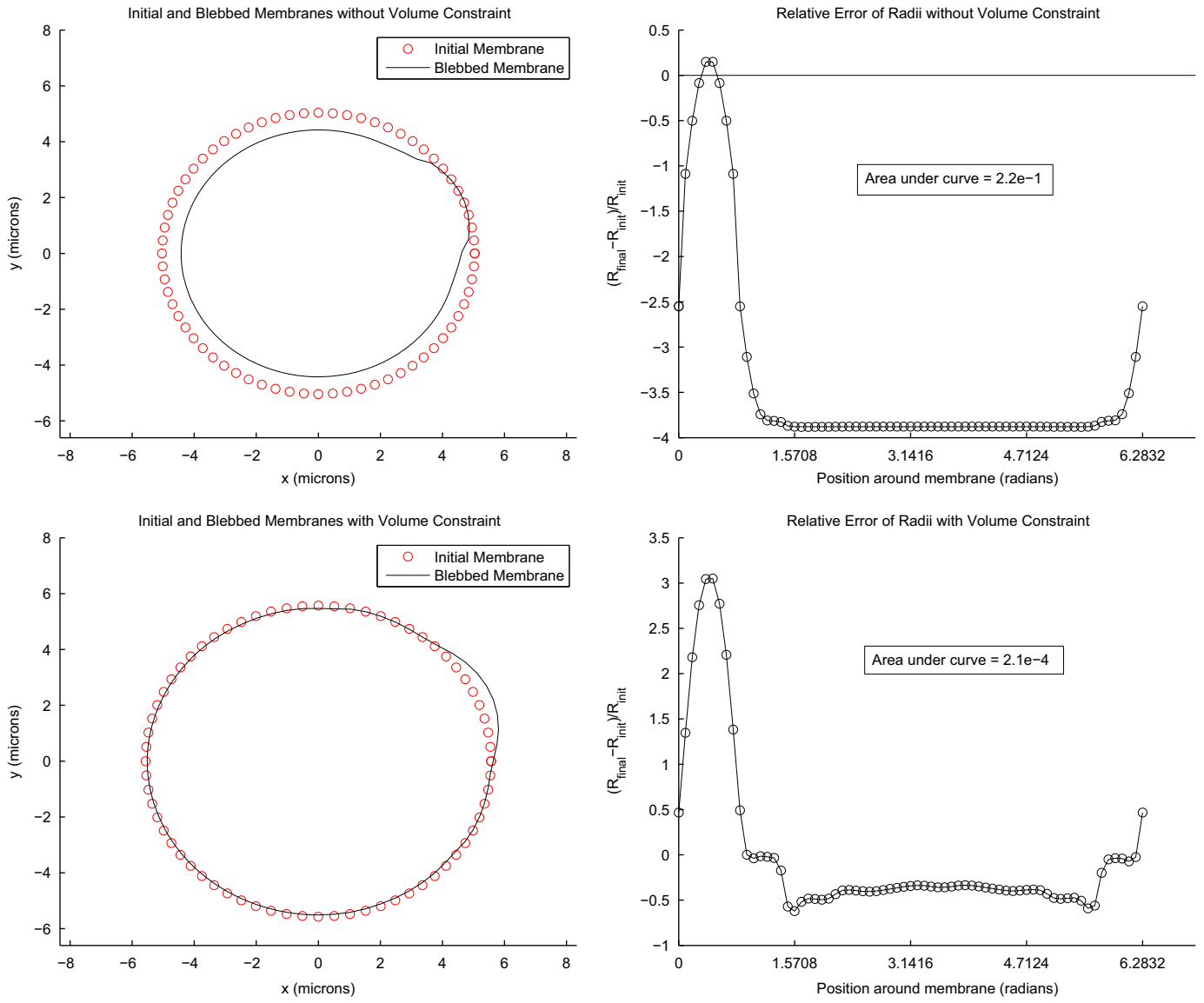

Fig. 9. In the left column, the dotted circles depicts the initial position of the membrane, while the solid line represents the membrane at a later time once blebbing has begun. The top figure does not have a volume constraint imposed, while the bottom one does. The two graphs to the right plot the relative error between the radii of the blebbed membrane versus the initial membrane with respect to position on the membrane. If volume is being conserved, the integral of the graph should be close to zero, which is for the bottom graph but not for the top graph.

no constraint there is clearly a decrease in volume, while in the volume constraint case although the bleb forms, the rest of the membrane adjusts to maintain the overall cell volume.

As a general validation of the overall model, the code was run using three levels of fluid grid discretization: 12×12, 24×24 and 48×48. We compared the perimeter and area of a bleb at different points in time given the same initial parameters for the three grids. The results are shown in Fig. 10.

4. Discussion

We have developed an entire-cell, fluid–structure interaction model of cellular blebbing. It is a first step in the construction of a continuum-microscopic framework, to be completed in subsequent work with a micromechanical computation of the cytoskeleton. The complex actin cortex micromechanics are represented here through average forces exerted through an equivalent elastic filament network. In the next stage of the model, the micromechanical computation will be used to more accurately update these average forces at each time step. We adopt a reductionist approach (Mogilner, 2009) in the construction of the computational model in which separate components are modeled individually. Some biologically relevant conclusions can already be drawn from the current computational model: (1) Bleb retraction is successfully predicted by the formation of a new cytoskeleton built from actin and myosin subunits, using accepted values for protein diffusivity and the computed advection velocity field. Also, the model simulates blebs of realistic geometric complexity. (2) The model constitutes an alternative to invoking complex continuum behavior for the cytoskeleton immersed in cytosol such as the poroelastic hypothesis of Charras et al. (2008). Localized in space and time stress non-uniformities are obtained in the model. Furthermore, these non-uniformities can readily be linked to detailed micromechanics of the cytoskeleton through the equivalent filament force concept introduced here. In contrast,

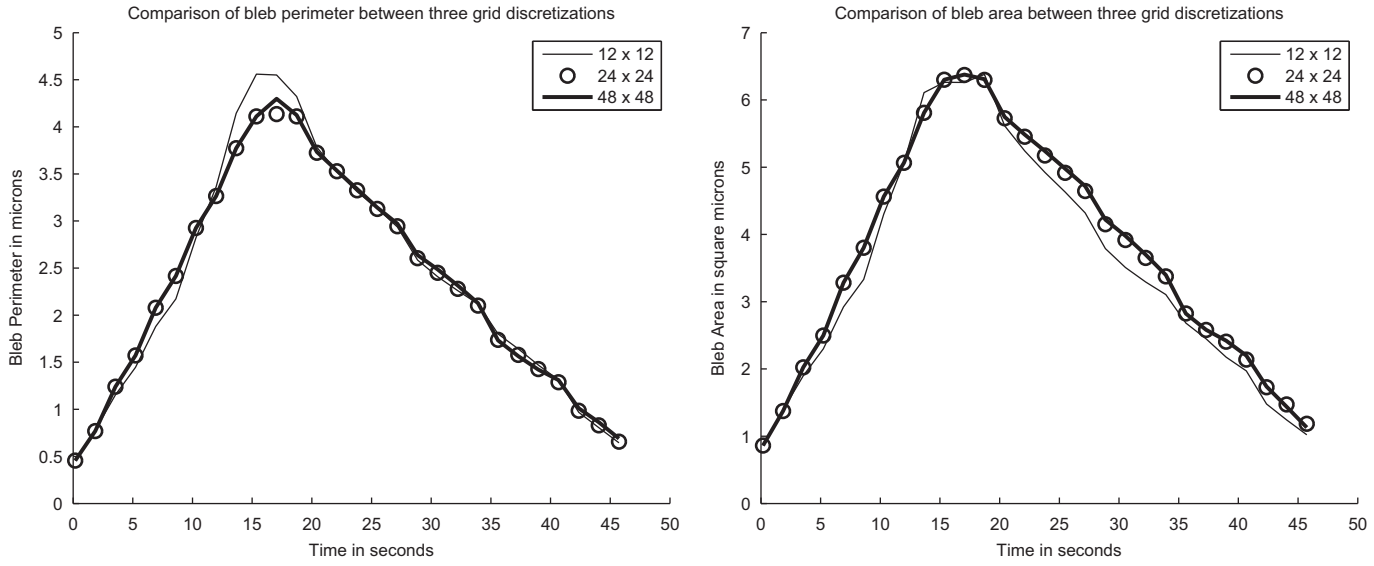

Fig. 10. These graphs show the evolution of the perimeter (left) and area (right) of a bleb over time for three grid discretizations using the same parameter set.

a complex, time-dependent constitutive law would be required in a poroelastic description of the cytoskeleton–cytosol ensemble. (3) The behavior of the membrane is realistically captured by a strain-dependent elasticity modulus as supported by scanning-force microscopy data (Künneke et al., 2004). Again, this modeling approach can more readily be linked to microscopic computations of membrane dynamics by comparison to a fluid mosaic model (Alberts et al., 2002). (4) The volume constraint present in the model ensures accurate computation of cytosol flow. In immersed interface or immersed boundary methods (Bottino and Fauci, 1998), the distributed singularity techniques often lead to small numerical fluid fluxes through the membrane which should be impermeable at the scale of the blebbing phenomenon. Though such errors tend to cancel out globally and have little effect on overall quantities (e.g. bleb volume), they would adversely affect local micromechanical and biochemical network descriptions like those we intend to add to the model. The least constraint step used in the algorithm we present here ensures that accurate fluid stress and velocity fields are obtained everywhere, even close to the membrane.

In the future, we plan to add more biological factors to the model such as levels of the membrane–cytoskeleton adhesive proteins. We are currently working on including a micromechanics model of the cytoskeleton to furnish the filament equivalent forces introduced in this model. The current work is a step in providing a software platform to answer quantitative questions about blebbing, one of the current challenges in computational biology (Mogilner, 2009).

Conflict of interest statement

The authors of this paper have no conflicts of interest related to this project.

Acknowledgments

This project developed after discussions with Dr. Timothy Elston, Dr. Kenneth Jacobson, and Dr. Gabriel Weinreb on modeling blebs. The research effort was partially supported by NIH Grant R01-HL077546-5401A2.

References

Alberts, B., Johnson, A., Lewis, J., Raff, M., Roberts, K., Walter, P., 2002. Molecular Biology of the Cell, fourth ed. Garland.
Albrecht-Buehler, G., 1982. Does blebbing reveal the convulsive flow of liquid and solutes through the cytoplasmic meshwork? Cold Spring Harbor Symposia on Quantitative Biology 46 (1), 45–49.
Alt, W., Dembo, M., 1999. Cytoplasm dynamics and cell motion: two-phase fluid models. Mathematical Biosciences 156 (1–2), 207–228.
Bak, J., Newman, D.J., 1997. Complex Analysis, second ed. Springer, Berlin.
Bertsekas, D.P., 1982. Constrained Optimization and Lagrange Multiplier Methods. Academic Press, New York.
Bicknese, S., Periasamy, N., Shohet, S.B., Verkman, A.S., 1993. Cytoplasmic viscosity near the cell plasma membrane: measurement by evanescent field frequency-domain microfluorimetry. Biophysical Journal 65 (3), 1272–1282.
Boal, D., 2002. Mechanics of the Cell. Cambridge University Press, Cambridge.
Bottino, D., Fauci, L., 1998. A computational model of ameboid deformation and locomotion. European Biophysics Journal 27 (5), 532–539.
Bray, D., 2000. Cell Movements: From Molecules to Motility, second ed. Garland.
Cano, M.L., Lauffenburger, D.A., Zigmond, S.H., 1991. Kinetic analysis of f-actin depolymerization in polymorphonuclear leukocyte lysates indicates that chemoattractant stimulation increases actin filament number without altering the filament length distribution. The Journal of Cell Biology 115, 677–687.
Charras, G.T., 2008. A short history of blebbing. Journal of Microscopy 231 (3), 466–478.
Charras, G.T., Coughlin, M., Mitchison, T.J., Mahadevan, L., 2008. Life and times of a cellular bleb. Biophysical Journal 94 (5), 1836–1853.
Charras, G.T., Hu, C., Coughlin, M., Mitchison, T.J., 2006. Reassembly of contractile actin cortex in cell blebs. The Journal of Cell Biology 175 (3), 477–490.
Charras, G.T., Yarrow, J.C., Horton, M.A., Mahadevan, L., Mitchison, T.J., 2005. Non-equilibration of hydrostatic pressure in blebbing cells. Nature 435, 365–369.
Cunningham, C.C., 1995. Actin polymerization and intracellular solvent flow in cell surface blebbing. The Journal of Cell Biology 129 (6), 1589–1599.
Dai, J., Sheetz, M.P., 1999. Membrane tether formation from blebbind cells. Biophysical Journal 77 (6), 3363–3370.
Dai, J., Sheetz, M.P., Wan, X., Morris, C.E., 1998. Membrane tension in swelling and shrinking molluscan neurons. The Journal of Neuroscience 18 (17), 6681–6692.
Erickson, C.A., Trinkaus, J.P., 1976. Microvilli and blebs as sources of reserve surface membrane during cell spreading. Experimental Cell Research 99 (2), 375–384.
Evans, E., Skalak, R., 1980. Mechanics and Thermodynamics of Biomembranes. CRC Press, Boca Raton.
Evans, E., Yeung, A., 1989. Apparent viscosity and cortical tension of blood granulocytes determined by micropipet aspiration. Biophysical Journal 56 (1), 151–160.
Fletcher, C.A.J., 1988. Computational Techniques for Fluid Dynamics: Volume 2, second ed. Springer, Berlin.

Herring, T.L., Cohan, C.S., Welnhofer, E.A., Mills, L.R., Morris, C.E., 1999. F-actin at newly invaginated membrane in neurons: implications for surface area regulation. Journal of Membrane Biology 171 (2), 151–169.
Janmey, P.A., Tang, J.X., Schmidt, C.F., Actin filaments, unpublished.
Jose, J.V., Saletan, E.J., 1998. Classical Dynamics: A Contemporary Approach. Cambridge University Press, Cambridge.
Keller, H., Eggli, P., 1998. Protrusive activity, cytoplasmic compartmentalization, and restriction rings in locomoting blebbing walker carcinosarcoma cells are related to detachment of cortical actin from the plasma membrane. Cell Motility and the Cytoskeleton 41 (2), 181–193.
Kolega, J., Taylor, D.L., 1993. Gradients in the concentration and assembly of myosin ii in living fibroblasts during locomotion and fiber transport. Molecular Biology of the Cell 4 (8), 819–836.
Künneke, S., Krüger, D., Janshoff, A., 2004. Scrutiny of the failure of lipid membranes as a function of headgroups, chain length, and lamellarity measured by scanning force microscopy. Biophysical Journal 86 (3), 1545–1553.
LeVeque, R., 1997. Wave propagation algorithms for multidimensional hyperbolic systems. Journal of Computational Physics 131, 327–353.
Mastro, A.M., Babich, M.A., Taylor, W.D., Keith, A.D., 1984. Diffusion of a small molecule in the cytoplasm of mammalian cells. Proceedings of the National Academy of Sciences of the United States of America 81 (11), 3414–3418.
Mills, J.C., Stone, N.L., Erhardt, J., Pittman, R.N., 1998. Apoptotic membrane blebbing is regulated by myosin light chain phosphorylation. The Journal of Cell Biology 140 (3), 627–636.
Mitran, S., 2001. Bearclaw. 〈http://coanda.amath.unc.edu/bearclaw〉.
Mogilner, A., 2009. Mathematics of cell motility: have we got its number? Journal of Mathematical Biology 58 (1–2), 105–134.
Morris, C.E., Homann, U., 2001. Cell surface area regulation and membrane tension. The Journal of Membrane Biology 179 (2), 79–102.
Nichol, J.A., Hutter, O.F., 1996. Tensile strength and dilatational elasticity of giant sarcolemmal vesicles shed from rabbit muscle. The Journal of Physiology 493 (1), 187–198.
Papastavridis, J.G., 2002. Analytical Mechanics: A Comprehensive Treatise on the Dynamics of Constrained Systems; For Engineers, Physicists, And Mathematicians. Oxford University Press, Oxford.
Pullarkat, P.A., 2006. Loss of cell–substrate adhesion leads to periodic shape oscillations in fibroblasts. eprint arXiv:physics/0612156.
Rand, R.P., Burton, A.C., 1964. Mechanical properties of the red cell membrane. I. Membrane stiffness and intracellular pressure. Biophysical Journal 4 (2), 115–135.
Rawicz, W., Olbrich, K.C., McIntosh, T., Needham, D., Evans, E., 2000. Effect of chain length and unsaturation on elasticity of lipid bilayers. Biophysical Journal 79 (1), 328–339.
Ryskin, G., Leal, L.G., 1983. Orthogonal mapping. Journal of Computational Physics 50, 71–100.
Schmid-Schönbein, G.W., Shih, Y.Y., Chien, S., 1980. Morphometry of human leukocytes. Blood 56 (5), 866–875.
Sheetz, M.P., 2001. Cell control by membrane–cytoskeleton adhesion. Nature Reviews. Molecular Cell Biology 2 (5), 392–396.
Sheetz, M.P., Sable, J.E., Döbereiner, H., 2006. Continuous membrane–cytoskeleton adhesion requires continuous accommodation to lipid and cytoskeleton dynamics. Annual Review of Biophysics and Biomolecular Structure 35, 417–434.
Yoon, Y., Kotar, J., Yoon, G., Cicuta, P., 2008. The nonlinear mechanical response of the red blood cell. Physical Biology 5 (3), 036007.
Zhang, Y., Jia, Y., Wang, S., 2006. 2d nearly orthogonal mesh generation with controls on distortion function. Journal of Computational Physics 218 (2), 549–571.
Zicha, D., Dobbie, I.M., Holt, M.R., Monypenny, J., Soong, D.Y.H., Gray, C., Dunn, G.A., 2003. Rapid actin transport during cell protrusion. Science 300 (5616), 142–145.